PRAMANA
— journal of
physics

Vol. 57, Nos 2 & 3
Aug. & Sept. 2001
pp. 355–369

First results from RHIC-PHENIX*

TARUN KANTI GHOSH[40]
For the PHENIX Collaboration

K Adcox,[40] S S Adler,[3] N Ajitanand,[27] Y Akiba,[14] J Alexander,[27] L Aphecetche,[34] Y Arai,[14] S H Aronson,[3] R Averbeck,[28] T C Awes,[29] K N Barish,[5] P D Barnes,[19] J Barrette,[21] B Bassalleck,[25] S Bathe,[22] V Baublis,[30] A Bazilevsky,[12,32] S Belikov,[12,13] F G Bellaiche,[29] S T Belyaev,[16] M J Bennett,[19] Y Berdnikov,[35] S Botelho,[33] M L Brooks,[19] D S Brown,[26] N Bruner,[25] D Bucher,[22] H Buesching,[22] V Bumazhnov,[12] G Bunce,[3,32] J Burward-Hoy,[28] S Butsyk,[28,30] T A Carey,[19] P Chand,[2] J Chang,[5] W C Chang,[1] L L Chavez,[25] S Chernichenko,[12] C Y Chi,[8] J Chiba,[14] M Chiu,[8] R K Choudhury,[2] T Christ,[28] T Chujo,[3,39] M S Chung,[15,19] P Chung,[27] V Cianciolo,[29] B A Cole,[8] D G D'Enterria,[34] G David,[3] H Delagrange,[34] A Denisov,[12] A Deshpande,[32] E J Desmond,[3] O Dietzsch,[33] B V Dinesh,[2] A Drees,[28] A Durum,[12] D Dutta,[2] K Ebisu,[24] Y V Efremenko,[29] K El Chenawi,[40] H En'yo,[17,31] S Esumi,[39] L Ewell,[3] T Ferdousi,[5] D E Fields,[25] S L Fokin,[16] Z Fraenkel,[42] A Franz,[3] A D Frawley,[9] S-Y Fung,[5] S Garpman,[20] T K Ghosh,[40] A Glenn,[36] A L Godoi,[33] Y Goto,[32] S V Greene,[40] M Grosse Perdekamp,[32] S K Gupta,[2] W Guryn,[3] H-Å Gustafsson,[20] J S Haggerty,[3] H Hamagaki,[7] A G Hansen,[19] H Hara,[24] E P Hartouni,[18] R Hayano,[38] N Hayashi,[31] X He,[10] T K Hemmick,[28] J Heuser,[28] J C Hill,[13] D S Ho,[43] K Homma,[11] B Hong,[15] A Hoover,[26] T Ichihara,[31,32] K Imai,[17,31] M S Ippolitov,[16] M Ishihara,[31,32] B V Jacak,[28,32] W Y Jang,[15] J Jia,[28] B M Johnson,[3] S C Johnson,[18,28] K S Joo,[23] S Kametani,[41] J H Kang,[43] M Kann,[30] S S Kapoor,[2] S Kelly,[8] B Khachaturov,[42] A Khanzadeev,[30] J Kikuchi,[41] D J Kim,[43] H J Kim,[43] S Y Kim,[43] Y G Kim,[43] W W Kinnison,[19] E Kistenev,[3] A Kiyomichi,[39] C Klein-Boesing,[22] S Klinksiek,[25] L Kochenda,[30] D Kochetkov,[5] V Kochetkov,[12] D Koehler,[25] T Kohama,[11] A Kozlov,[42] P J Kroon,[3] K Kurita,[31,32] M J Kweon,[15] Y Kwon,[43] G S Kyle,[26] R Lacey,[27] J G Lajoie,[13] J Lauret,[27] A Lebedev,[13] D M Lee,[19] M J Leitch,[19] X H Li,[5] Z Li,[6,31] D J Lim,[43] M X Liu,[19] X Liu,[6] Z Liu,[6] C F Maguire,[40] J Mahon,[3] Y I Makdisi,[3] V I Manko,[16] Y Mao,[6,31] S K Mark,[21] S Markacs,[8] G Martinez,[34] M D Marx,[28] A Masaike,[17] F Matathias,[28] T Matsumoto,[7,41] P L McGaughey,[19] E Melnikov,[12] M Merschmeier,[22] F Messer,[28] M Messer,[3] Y Miake,[39] T E Miller,[40] A Milov,[42] S Mioduszewski,[3,36] R E Mischke,[19] G C Mishra,[10] J T Mitchell,[3] A K Mohanty,[2] D P Morrison,[3] J M Moss,[19] F Mühlbacher,[28] M Muniruzzaman,[5] J Murata,[31] S Nagamiya,[14] Y Nagasaka,[24] J L Nagle,[8] Y Nakada,[17] B K Nandi,[5] J Newby,[36] L Nikkinen,[21] P Nilsson,[20] S Nishimura,[7] A S Nyanin,[16] J Nystrand,[20] E O'Brien,[3] C A Ogilvie,[13] H Ohnishi,[3,11] I D Ojha,[4,40] M Ono,[39] V Onuchin,[12] A Oskarsson,[20] L Österman,[20] I Otterlund,[20] K Oyama,[7,38] L Paffrath,[3,*] A P T Palounek,[19] V S Pantuev,[28] V Papavassiliou,[26] S F Pate,[26] T Peitzmann,[22] A N Petridis,[13] C Pinkenburg,[3,27] R P Pisani,[3] P Pitukhin,[12] F Plasil,[29] M Pollack,[28,36] K Pope,[36] M L Purschke,[3] I Ravinovich,[42] K F Read,[29,36] K Reygers,[22] V Riabov,[30,35] Y Riabov,[30] M Rosati,[13] A A Rose,[40] S S Ryu,[43] N Saito,[31,32] A Sakaguchi,[11]

*The word PHENIX is the abbreviation of Pioneering High Energy Nuclear Interaction Experiment.

T Sakaguchi,[7,41] H Sako,[39] T Sakuma,[31,37] V Samsonov,[30] T C Sangster,[18] R Santo,[22] H D Sato,[17,31] S Sato,[39] S Sawada,[14] B R Schlei,[19] Y Schutz,[34] V Semenov,[12] R Seto,[5] T K Shea,[3] I Shein,[12] T-A Shibata,[31,37] K Shigaki,[14] T Shiina,[19] Y H Shin,[43] I G Sibiriak,[16] D Silvermyr,[20] K S Sim,[15] J Simon-Gillo,[19] C P Singh,[4] V Singh,[4] M Sivertz,[3] A Soldatov,[12] R A Soltz,[18] S Sorensen,[29,36] P W Stankus,[29] N Starinsky,[21] P Steinberg,[8] E Stenlund,[20] A Ster,[44] S P Stoll,[3] M Sugioka,[31,37] T Sugitate,[11] J P Sullivan,[19] Y Sumi,[11] Z Sun,[6] M Suzuki,[39] E M Takagui,[33] A Taketani,[31] M Tamai,[41] K H Tanaka,[14] Y Tanaka,[24] E Taniguchi,[31,37] M J Tannenbaum,[3] J Thomas,[28] J H Thomas,[18] T L Thomas,[25] W Tian,[6,36] J Tojo,[17,31] H Torii,[17,31] R S Towell,[19] I Tserruya,[42] H Tsuruoka,[39] A A Tsvetkov,[16] S K Tuli,[4] H Tydesjö,[20] N Tyurin,[12] T Ushiroda,[24] H W van Hecke,[19] C Velissaris,[26] J Velkovska,[28] M Velkovsky,[28] A A Vinogradov,[16] M A Volkov,[16] A Vorobyov,[30] E Vznuzdaev,[30] H Wang,[5] Y Watanabe,[31,32] S N White,[3] C Witzig,[3] F K Wohn,[13] C L Woody,[3] W Xie,[5,42] K Yagi,[39] S Yokkaichi,[31] G R Young,[29] I E Yushmanov,[16] W A Zajc,[8] Z Zhang,[28] and S Zhou[6]

[1]Institute of Physics, Academia Sinica, Taipei 11529, Taiwan
[2]Bhabha Atomic Research Centre, Mumbai 400 085, India
[3]Brookhaven National Laboratory, Upton, NY 11973-5000, USA
[4]Department of Physics, Banaras Hindu University, Varanasi 221005, India
[5]University of California - Riverside, Riverside, CA 92521, USA
[6]China Institute of Atomic Energy (CIAE), Beijing, People's Republic of China
[7]Center for Nuclear Study, Graduate School of Science, University of Tokyo, 7-3-1 Hongo, Bunkyo, Tokyo 113-0033, Japan
[8]Columbia University, New York, NY 10027 and Nevis Laboratories, Irvington, NY 10533, USA
[9]Florida State University, Tallahassee, FL 32306, USA
[10]Georgia State University, Atlanta, GA 30303, USA
[11]Hiroshima University, Kagamiyama, Higashi-Hiroshima 739-8526, Japan
[12]Institute for High Energy Physics (IHEP), Protvino, Russia
[13]Iowa State University, Ames, IA 50011, USA
[14]KEK, High Energy Accelerator Research Organization, Tsukuba-shi, Ibaraki-ken 305-0801, Japan
[15]Korea University, Seoul, 136-701, Korea
[16]Russian Research Center "Kurchatov Institute", Moscow, Russia
[17]Kyoto University, Kyoto 606, Japan
[18]Lawrence Livermore National Laboratory, Livermore, CA 94550, USA
[19]Los Alamos National Laboratory, Los Alamos, NM 87545, USA
[20]Department of Physics, Lund University, Box 118, SE-221 00 Lund, Sweden
[21]McGill University, Montreal, Quebec H3A 2T8, Canada
[22]Institut fuer Kernphysik, University of Muenster, D-48149 Muenster, Germany
[23]Myongji University, Yongin, Kyonggido 449-728, Korea
[24]Nagasaki Institute of Applied Science, Nagasaki-shi, Nagasaki 851-0193, Japan
[25]University of New Mexico, Albuquerque, NM, USA
[26]New Mexico State University, Las Cruces, NM 88003, USA
[27]Chemistry Department, State University of New York - Stony Brook, Stony Brook, NY 11794, USA
[28]Department of Physics and Astronomy, State University of New York - Stony Brook, Stony Brook, NY 11794, USA
[29]Oak Ridge National Laboratory, Oak Ridge, TN 37831, USA
[30]PNPI, Petersburg Nuclear Physics Institute, Gatchina, Russia
[31]RIKEN (The Institute of Physical and Chemical Research), Wako, Saitama 351-0198, Japan
[32]RIKEN BNL Research Center, Brookhaven National Laboratory, Upton, NY 11973-5000, USA
[33]Universidade de São Paulo, Instituto de Física, Caixa Postal 66318, São Paulo CEP05315-970, Brazil
[34]SUBATECH (Ecole des Mines de Nantes, IN2P3/CNRS, Universite de Nantes) BP 20722-44307, Nantes-cedex 3, France
[35]St Petersburg State Technical University, St Petersburg, Russia
[36]University of Tennessee, Knoxville, TN 37996, USA

[37]Department of Physics, Tokyo Institute of Technology, Tokyo, 152-8551, Japan
[38]University of Tokyo, Tokyo, Japan
[39]Institute of Physics, University of Tsukuba, Tsukuba, Ibaraki 305, Japan
[40]Vanderbilt University, Nashville, TN 37235, USA
[41]Waseda University, Advanced Research Institute for Science and Engineering, 17 Kikui-cho, Shinjuku-ku, Tokyo 162-0044, Japan
[42]Weizmann Institute, Rehovot 76100, Israel
[43]Yonsei University, IPAP, Seoul 120-749, Korea
[44]Individual Participant: KFKI Research Institute for Particle and Nuclear Physics (RMKI), Budapest, Hungary

Abstract. The PHENIX experiment consists of a large detector system located at the newly commissioned relativistic heavy ion collider (RHIC) at the Brookhaven National Laboratory. The primary goal of the PHENIX experiment is to look for signatures of the QCD prediction of a deconfined high-energy-density phase of nuclear matter quark gluon plasma. PHENIX started data taking for Au+Au collisions at $\sqrt{s_{NN}} = 130$ GeV in June 2000. The signals from the beam-beam counter (BBC) and zero degree calorimeter (ZDC) are used to determine the centrality of the collision. A Glauber model reproduces the ZDC spectrum reasonably well to determine the participants in a collision. Charged particle multiplicity distribution from the first PHENIX paper is compared with the other RHIC experiment and the CERN, SPS results. Transverse momentum of photons are measured in the electro-magnetic calorimeter (EMCal) and preliminary results are presented. Particle identification is made by a time of flight (TOF) detector and the results show clear separation of the charged hadrons from each other.

Keywords. Relativistic heavy ions; quark gluon plasma; PHENIX.

PACS Nos 25.75.-q; 24.85.+p

1. Introduction

PHENIX is a large detector experiment [1] at the newly comissioned relativistic heavy ion collider (RHIC) at the Brookhaven National Laboratory. The relativistic heavy ion collider (RHIC) started operation in June 2000. The PHENIX experiment started to collect data simultaneously with three other experiments namely STAR, PHOBOS, and BRAHMS. The detector subsystems in PHENIX are designed to measure signals from hadrons, leptons, and photons produced in the nucleus–nucleus, and proton–proton collisions at beam energies up to 100 GeV/A. The primary motivation for this experiment is to look for the signatures from the nuclear matter at the highest temperatures and energy densities. This high density phase of matter is predicted to be the quark gluon plasma.

According to Bjorken [2], the spatial energy density (ϵ) in a relativistic collision can be deduced by measuring the transverse energy density in rapidity, $\mathrm{d}E_{\mathrm{T}}/\mathrm{d}y$, which is effectively the co-moving energy density in a longitudinal expansion:

$$\epsilon_{Bj} = \frac{\mathrm{d}E_{\mathrm{T}}}{\mathrm{d}y}\frac{1}{2\tau_0\pi R^2}, \tag{1}$$

where τ_0, the formation time, is usually taken as $\frac{1}{2}$ fm/c, and πR^2 is the effective area of the collision.

There are two important properties of the plasma. Observation of Debye screening of quantum chromodynamics (QCD) interactions and confirmation of chiral symmetry restoration, are significant goals of PHENIX measurements. The thermal radiation of a

hot gas is also extremely important; it characterizes the temperature of the system formed in these collisions. The strategy behind PHENIX is to study both lepton and hadron signatures in the same experiment. The leptons arise from the plasma phase and probe it directly whereas the more copious hadrons provide the complementary information about the hadronization phase transition. To study the above physics quantities, electron pairs, muon pairs, photons and charged hadrons must be measured. Electron and muon pairs are measured to study properties of the vector mesons and also to study the continuum spectra in different regions of rapidity and mass. The electron and muon coincidence probes charm production and aids in understanding the shape of continuum dilepton spectra. Photon measurements probe the initial phase via the prompt photons. Measurements of collective flow, in particular elliptical flow has been predicted to get the crucial information about the equation of state (EOS) [19–21] of the nuclear matter. In a recent paper [22], it has been predicted that for non-central collisions at RHIC energy there may be an unusual exapansion which can not be described by simply an elliptical flow. The type of flow at RHIC may be qualitatively different than the flow observed at AGS/SPS [23,26] energies. PHENIX has the capability to measure the azimuthal correlations and elliptical flow at the mid-rapidity. Detection and identification of charged hadrons allow study of the P_{T} distributions, production of anti-nuclei, the ϕ meson (via K^+K^- decay), jets, elliptical flow, and Hanbury–Brown–Twiss (HBT) correlations. The PHENIX detector is designed to measure these particles in both the forward and mid-rapidity regions and to have good particle identification capability to distinguish the different types of particles. Of particular interest to PHENIX are the signals corresponding to the decay of vector mesons into lepton pairs, which are detected in the electron and muon arms, respectively, of the PHENIX detector. The detector performance is optimized to detect the lepton pairs and photons with good efficiency over a large momentum range. In this paper we will limit discussion to the measurment of the multiplicity distribution and transverse energy distribution in the mid rapidity and their impacts on the energy density. We will also discuss the preliminary plots of particle identification from the PHENIX time-of-flight (TOF) detector and the measurements of elliptical flow at the mid-rapidity from the charged tracks measured by PHENIX central arm detectors.

2. Detector setup

The PHENIX detector consists of two arms around an axial central magnet and two muon endcaps along the beamlines as shown in figure 1. The central arms are being instrumented to detect electrons, photons and hadrons in the zero rapidity region and the muon arms are optimized for detection of dimuons in the forward-rapidity region.

The detector subsystems can be classified into three categories. The first category are the inner detectors consisting of the silicon multiplicity and vertex detector (MVD) of strip and pad types, arranged around the interaction region and a pair of beam-beam counters (BBC) placed close to beam direction on either side of the vertex for detecting particles produced at glancing angles. The second category are the central arm detectors in 90 degree East and West azimuthal sectors. This group consists of: an intermediate tracker (ITR) made of drift chambers (DCH) and pad chambers (PC1), a ring imaging Cerenkov detector (RICH), an outer tracker comprised of two pad chambers (PC2, PC3) before and after a time-expansion chambers (TEC), a time-of-flight scintillators (TOF), and an electromagnetic calorimeter (EMCal) of the lead-scintillator type in a shish-kebab structure and also a sector of lead glass detectors, both coupled to photomultiplier. For the run2000 PHENIX used PC1 and

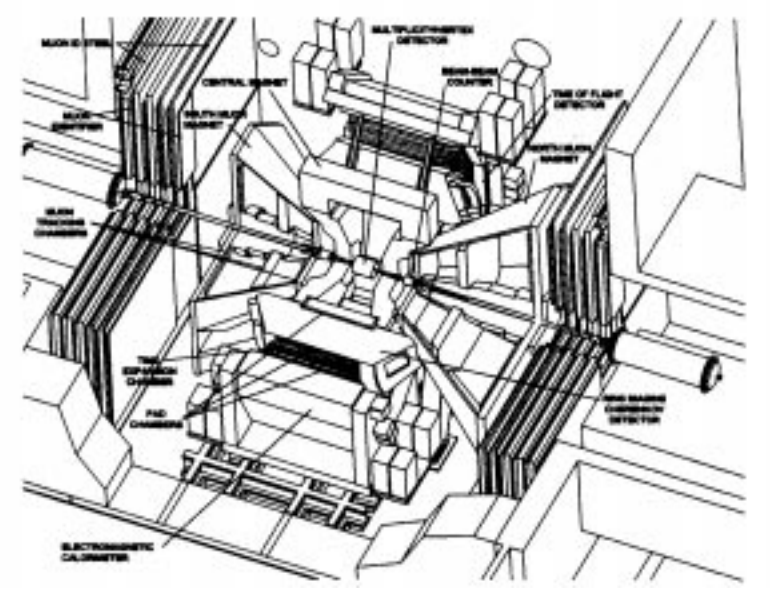

Figure 1. PHENIX detector setup.

PC3 in the east arm and only PC1 in the West arm. The third category are the two muon arms, North and South, each consisting of three tracking stations, and a muon identifier subsystem covering the forward rapidity. The muon arms were not used in the year 2000 data taking.

The beam-beam counter (BBC) provides information for triggering on beam-beam collisions and obtains the collision vertex position (resolution around 2 cm) along the beam axis that helps to find correlation between tracks in various detector elements and the time origin of the collisions. The information must be available at the trigger level to discriminate backgrounds. The timing information is used to perform the time of flight measurement for particle identification combined with the information from the TOF detectors. The BBC consists of two arrays of counter elements, one each placed upstream and downstream of the beam crossing point. Each array consists of 64 modules of counter elements which are constructed from a Cerenkov radiator of fused quartz 3 cm long and photomultiplier tube (PMT) of $1''$ diameter. The average and difference of the arrival times of the fast leading charged particles from beam-beam collisions to the two BBC arrays provide the time origin and the vertex position of the collision.

The multiplicity and vertex detector (MVD), which is placed just outside the beam pipe, provides centrality trigger and more accurate vertex information. The MVD is comprised of two parts: two end caps and two concentric central barrel covered with silicon pads and strips. Vertex finding can be done with good efficiency using the hits from the central barrels for z-position up to ± 40 cm with a position resolution < 2 mm. The disk shaped end caps, located at z-positions of ± 35 cm, are composed of silicon pads. Analog sums of the signal from the end caps and also from the central barrel, allow formation of multiplicity triggers from different ranges of pseudorapidity.

The central arm tracking begins with a low mass, multiwire focusing drift chambers that (DC) provide high resolution P_{T} measurements. The pad chambers provide a three dimensional position measurement to aid in pattern recognition and to determine P_z/P_{T}. A six layer time expansion chamber (TEC) is located between PC2 and PC3. It assists in pattern recognition and provide electron pion separation from energy loss $(\mathrm{d}E/\mathrm{d}x)$ information. In future, the TEC will be upgraded to detect transition radiation X-rays.

The year 2000 measurement uses an electromagnetic lead/scintillating tile calorimeter which forms part of the PHENIX detector. The EMCal covers the pseudorapidity range $|\eta| \leq 0.38$ with an azimuthal aperture of $\Delta\phi = 180$ degrees. It is subdivided into 8 equal coverage sectors. Six sectors are lead/scintillator (PbSc) sampling calorimeters custom developed and built for PHENIX [3,4]; two sectors are lead–glass Cherenkov calorimeters (PbGl) imported from the WA98 experiment at CERN [6]. The PHENIX lead/scintillator EMCal is a shashlik type detector which is built of identical rectangular read-out towers 5.535×5.535 cm^2 in cross section. The depth of the calorimeter corresponds to 18 radiation lengths (X_0) and 0.85 interaction lengths. The calorimeter has a nominal energy resolution of $8\%/\sqrt{E(\mathrm{GeV})}$ and good intrinsic timing resolution $\sim$ 200 ps. The calorimeter response is proportional to incident electron energy to within $\pm 2\%$ over the range $0.3 \leq E_e \leq 40.0$ GeV.

3. Discussion on first RHIC-PHENIX run

There are two rings at RHIC and the machine is 2.4 miles around. The beam in both rings were accelerated with minimal transition losses to $\gamma = 70$ ($E = 65$ GeV/u) during this run. PHENIX saw the first collision on 15 June 2000 and the first run ended on 04 September 2000. During this run period PHENIX recorded $\sim$5 M minimum bias events from the Au–Au collisions at $\sqrt{s_{NN}} = 130$ GeV. RHIC ran only 28 MHz 'accelerating' RF in this run period and that results in the beam spread $\sigma = 50-70$ cm in the collision region.

4. Discussion on first PHENIX results

One of the important thing to determine in a heavy-ion collision is the centrality of the collision and number of participants in that collision. So first we begin with explaining how these determinations are accomplished in PHENIX. The upper panel of figure 2 is the correlation plot of analog response signals between zero degree calorimeters (ZDC) and beam-beam counters (BBC). Higher signals in the ZDC corresponds to lower centrality and so this plot can be used for the centrality selection of the events. Different slices represent different centrality bins. Each slice contains 5% of the total interaction cross section of 7.2 barns. Simulations of the BBC and ZDC response were done to account for the effect of physics and detector fluctuations in the definition of event classes and to relate them via a Glauber model [5] to the number of participating nucleons N_p and of binary collisions N_c. The average charged particle density is scaled up to one unit of rapidity and the corresponding number is $N_p = 347 \pm 10$ for the most central collisions [32]. The distribution in the bottom panel of figure 2 is the charged-particle multiplicity distribution at mid-rapidity, as measured by the PHENIX pad chambers (PC). Particle density at mid-rapidity is an essential global variable for the characterization of high energy nuclear collisions, providing information about the initial conditions, such as energy density. We

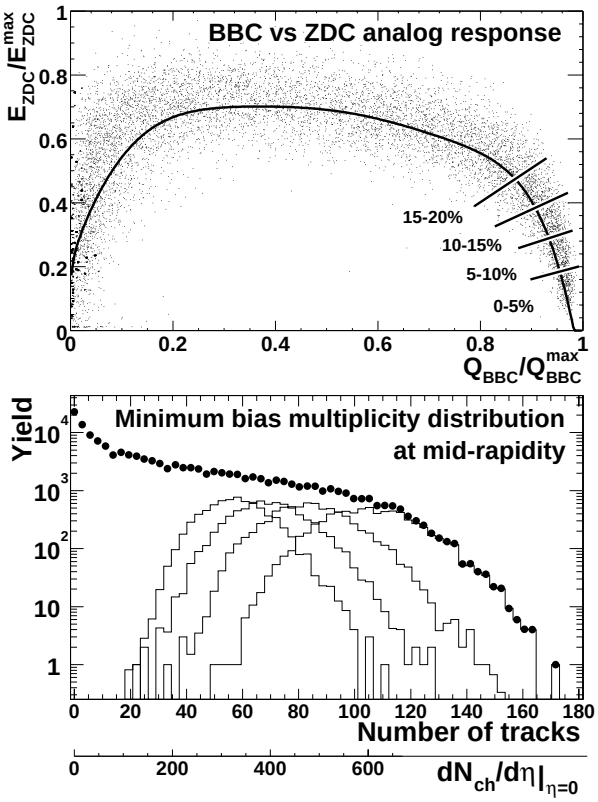

Figure 2. BBC vs ZDC analog response (top panel) and minimum-bias multiplicity distribution in the PHENIX measurement aperture (lower panel). The lower axis converts the observed distribution to the corresponding average $\mathrm{d}N_{\mathrm{ch}}/\mathrm{d}\eta$ for track multiplicities less than ~ 120; beyond that value the shape of the distribution has a significant contribution from fluctuations into the measurement aperture.

analyse the particle density as a function of centrality, expressed by the number of participating nucleons. Such an analysis may shed light on the relative importance of soft versus hard processes of particle production and test the assumption of gluon saturation expected at RHIC energies [10,11]. Our results are compared to different models, to similar studies obtained in Pb–Pb collisions at the CERN SPS [6,7,9] and to a recent measurement performed at RHIC by PHOBOS [8]. After applying the corrections we obtain in the lower panel of figure 2 the minimum-bias charged-particle multiplicity distribution, in the track acceptance $|\eta| < 0.35$, $\delta\phi = 88.4°$. A factor of 5.82 converts the observed number of tracks to $\mathrm{d}N_{\mathrm{ch}}/\mathrm{d}\eta_{|\eta=0}$ in one unit of pseudo-rapidity and full azimuth, yielding the lower horizontal scale in figure 2. The PHOBOS experiment has recently reported an average $\mathrm{d}N_{\mathrm{ch}}/\mathrm{d}\eta_{|\eta=0} = 555 \pm 12$ (stat) ± 35 (syst) for the 6% most central collisions [8]. For the same centrality bin, we find $\mathrm{d}N_{\mathrm{ch}}/\mathrm{d}\eta_{|\eta=0} = 609 \pm 1$ (stat) ± 37 (syst). From the preliminary results reported by NA49 in Pb–Pb collisions at $\sqrt{s_{_{NN}}} = 17.2$ GeV [9], we derive a particle density $\mathrm{d}N_{\mathrm{ch}}/\mathrm{d}y_{|y=0} = 410$. Our result, $\mathrm{d}N_{\mathrm{ch}}/\mathrm{d}\eta_{|\eta=0} = 622$ for the same centrality bin (0–5%), represents an increase of $\sim 80\%$ after scaling it by 1.2 to account for the

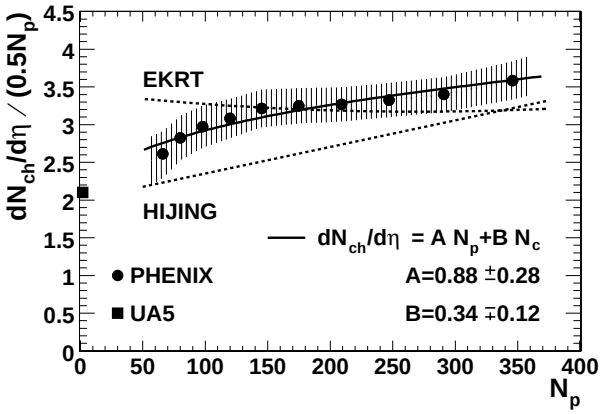

Figure 3. Charged-particle pseudo-rapidity density per participant pair vs the number of participants. Predictions from HIJING [10] and EKRT [11] models, and a simple phenomenological fit are also shown. The shaded area represents the systematic errors of $\mathrm{d}N_{\mathrm{ch}}/\mathrm{d}\eta$ and N_p.

transformation from η to y. We show in figure 3 our results for $\mathrm{d}N_{\mathrm{ch}}/\mathrm{d}\eta$ per participant pair as a function of the number of participants N_p. Figure 3 also shows the $p\overline{p}$ value at the same $\sqrt{s}$ taken from the UA5 analysis [31]. It is interesting to note that the extrapolation of our data points to low multiplicities approaches the $p\overline{p}$ value. A good fit to our data by functional form $\mathrm{d}N_{\mathrm{ch}}/\mathrm{d}\eta \propto N_p^{\alpha}$ gives the value $\alpha = 1.16 \pm 0.04$ which is higher than the CERN experiments. WA98 finds a best fit value of $\alpha = 1.07 \pm 0.04$ [6]. Experiment WA97 quotes a value $\alpha = 1.05 \pm 0.05$, consistent with the result of WA98. Other models such as the EKRT [11] predicts that at RHIC energies, the large production of semi-hard gluons in a small volume may saturate the gluon density. The resulting gluon fusion limits the total entropy production and thus lowers the final particle production per participant. The predictions of the EKRT model are also shown in figure 3. We observe no such saturation effect within our errors for Au+Au collisions at $\sqrt{s_{_{NN}}} = 130$ GeV, but instead see a steady rise in the particle production per participant pair. Model such as HIJING predicts that there is a component of particle production from soft interactions that scales linearly with N_p and a second component from hard processes (pQCD jets) that scales with N_c. Following that, we fit the data of figure 3 with the function $\mathrm{d}N_{\mathrm{ch}}/\mathrm{d}\eta = A \times N_p + B \times N_c$ using the values of N_c and N_p calculated from Glauber model. The results of the fit are shown in figure 3. The values of A and B imply a large contribution of hard processes to particle production. HIJING predicts the same trend although the calculated values are lower than the data by $\sim$15%.

The spectrum of the measured transverse energy from the PHENIX EMCal is shown in figure 4. The solid curve is for the minimum bias data sample and the dotted curves are for the four different centrality bins. The measurement is done at $\Delta\phi = 44.4^{\circ}$ azimuthal and $\Delta\eta = 0.76$ polar angle acceptance. The scaling transformation from the raw measured transverse energy, $E_{\mathrm{T\,EMC}}$, to the nominal hadronic $\mathrm{d}E_{\mathrm{T}}/\mathrm{d}\eta|_{\eta=0}$ involves correction for detector response, acceptance, inactive area, albedo from magnet poles and it amounts about a factor of 12.8 higher than the measured value. Mid-rapidity E_{T} distributions are a standard method of defining centrality [12,6,13,15].

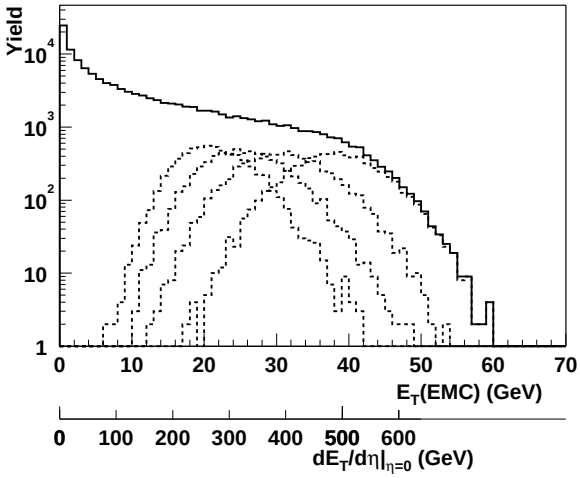

Figure 4. The $E_{\mathrm{T\,EMC}}$ distribution measured in the $\Delta\phi = 44.4^{\circ}$ azimuthal and $\Delta\eta = 0.76$ polar angle acceptance at $\sqrt{s_{NN}} = 130$ GeV. The lower scale represents a correction of the upper $E_{\mathrm{T\,EMC}}$ scale by a factor of 1.28 (see text) to correspond to the nominal total hadronic $\mathrm{d}E_{\mathrm{T}}/\mathrm{d}\eta|_{\eta=0}$ in the full azimuth. The solid line is the minimum bias distribution with the BBC trigger, the dotted lines correspond to centrality cuts as discussed in the text.

Thus, it is important to try to determine for the present data the detailed relationship of transverse energy production to the number of participants (N_{part}) in the nuclear collision. Figure 4 shows the $\mathrm{d}E_{\mathrm{T}}/\mathrm{d}\eta|_{\eta=0}$ distributions for the 4 most central ranges and the centrality bins are the same as it was previously discussed for the multiplicity distribution.

Figure 5 (left) shows that $\langle \mathrm{d}E_{\mathrm{T}}/\mathrm{d}\eta|_{\eta=0}\rangle$ per participant also increases with N_{part}. It also shows that $\langle \mathrm{d}E_{\mathrm{T}}/\mathrm{d}\eta|_{\eta=0}\rangle$ for central Au+Au collisions at $\sqrt{s_{NN}} = 130$ GeV is about 40% larger than found by WA98 in Pb+Pb at $\sqrt{s_{NN}} = 17.2$ GeV. The mid-rapidity E_{T} measurement of the NA49 collaboration for Pb+Pb collisions [15] at $\sqrt{s_{NN}} = 17.2$ GeV gives a value of $\mathrm{d}E_{\mathrm{T}}/\mathrm{d}\eta|_{\eta=0} = 405$ GeV for the most central 2% of the inelastic cross section, in excellent agreement with the WA98 value of 399 GeV for the same conditions. NA49 derives a value of $\epsilon_{Bj} = 3.2$ GeV/fm^3 at $\sqrt{s_{NN}} = 17.2$ GeV from this result. A straightforward derivation of ϵ_{Bj} from our measured $\mathrm{d}E_{\mathrm{T}}/\mathrm{d}\eta|_{\eta=0}$ of 578^{+29}_{-41} GeV for the same centrality cut, corrected to $\mathrm{d}E_{\mathrm{T}}/\mathrm{d}y|_{y=0}$ by a factor of 1.19 from our Monte Carlo, and taking πR^2=139 fm^2 from our Glauber calculation [5], gives $\epsilon_{Bj} = 5.0$ GeV/fm^3, an increase of more than 50% over the NA49 value.

This is better illustrated in figure 5 (right) where the ratio $\langle \mathrm{d}E_{\mathrm{T}}/\mathrm{d}\eta|_{\eta=0}\rangle / \langle \mathrm{d}N_{\mathrm{ch}}/\mathrm{d}\eta|_{\eta=0}\rangle$ remains constant at a value of ~ 0.8 GeV, in striking agreement both in absolute value and centrality (in)dependence with the measurements by WA98 [6] from Pb+Pb collisions at $\sqrt{s_{NN}} = 17.2$ GeV. The WA98 data for $\langle \mathrm{d}E_{\mathrm{T}}/\mathrm{d}\eta|_{\eta=0}\rangle$ per participant are shown in figure 5 (left) and are essentially independent of N_{part} for $N_{\mathrm{part}} > 200$. WA98 parameterizes their data as $\mathrm{d}E_{\mathrm{T}}/\mathrm{d}\eta|_{\eta=0} \propto N^{\alpha}_{\mathrm{part}}$ with $\alpha = 1.08 \pm 0.06$ while the same parameterization for our data yields $\alpha = 1.13 \pm 0.05$.

The particle identification of charged hadrons is performed by combining the information from the Drift Chamber, PC1, BBC, and TOF. The time of flight is an array of 960

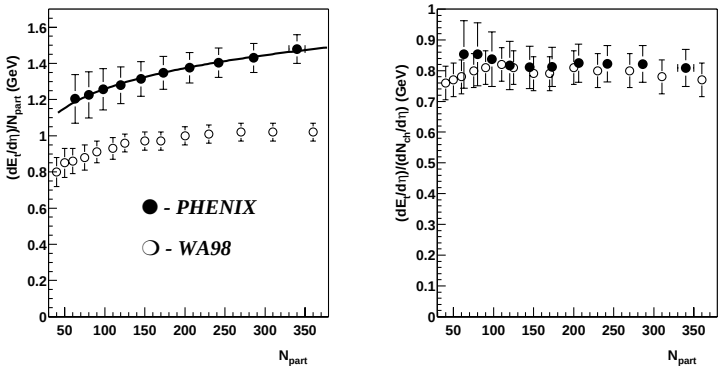

Figure 5. (Left) PHENIX transverse energy density per participant $\langle \mathrm{d}E_{\mathrm{T}}/\mathrm{d}\eta|_{\eta=0}\rangle/N_{\mathrm{part}}$ as a function of N_{part}, the number of participants in Au+Au collisions at $\sqrt{s_{NN}} = 130$ GeV compared to data from WA98 [6] for Pb+Pb collisions at $\sqrt{s_{NN}} = 17.2$ GeV. (Right) PHENIX $\langle \mathrm{d}E_{\mathrm{T}}/\mathrm{d}\eta|_{\eta=0}\rangle/\langle \mathrm{d}N_{\mathrm{ch}}/\mathrm{d}\eta|_{\eta=0}\rangle$ versus N_{part} compared to WA98 data.

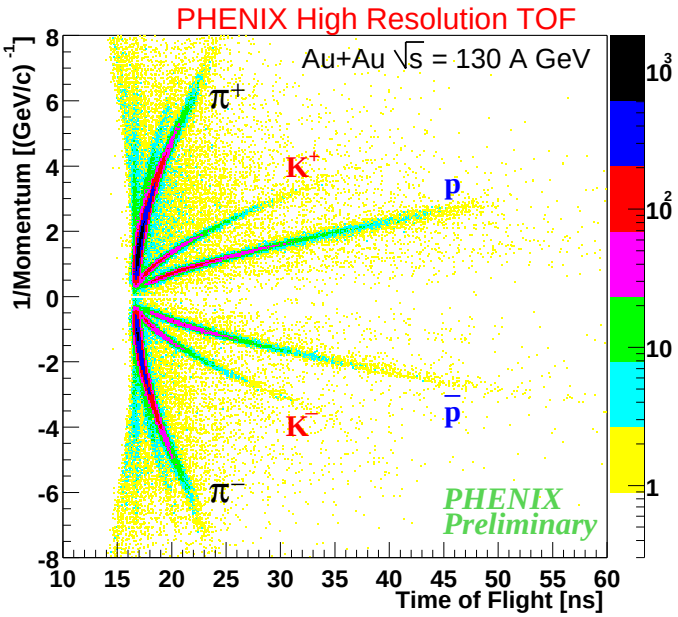

Figure 6. Contour plot of time-of-flight versus inverse momentum for minimum bias Au+Au collisions. This clearly demonstrates the capability of particle identification by time-of-flight detector in the year 2000 run of PHENIX experiment.

slats and each of the slat is connected with a photo multiplier tube (PMT) for the readout. The time resolution is 115 ps and it has the capacity of π/K separation at momenta up to 2.4 GeV/c and K/proton separation up to 4.0 GeV/c as shown in figure 6.

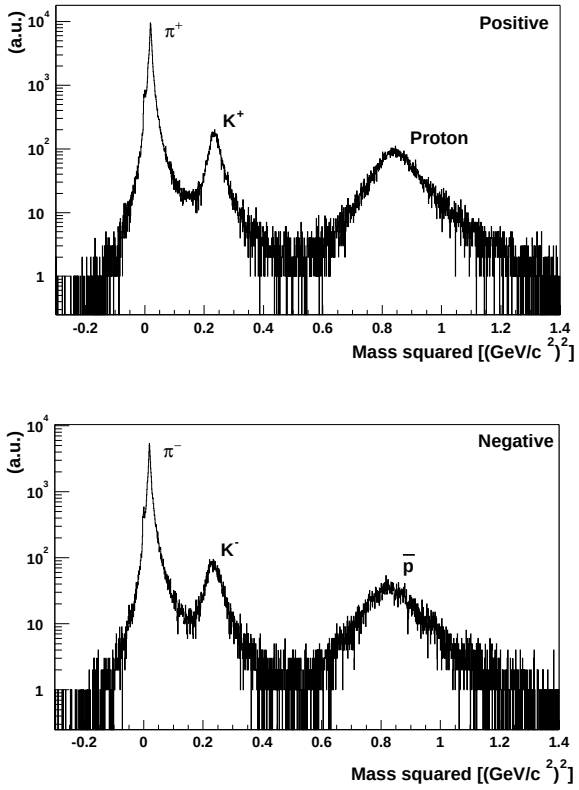

Figure 7. Squared mass distribution for (**a**) positively and (**b**) negatively charged particles measured by time-of-flight detector.

Once a global track is reconstructed using the Drift Chamber, PC1 and TOF, the flight path length of the track from the event vertex to the TOF is calculated and then that is used to correct the value of time-of-flight measured by TOF. Figure 6 shows a contour plot of the corrected time-of-flight value as a function of reciprocal momentum for minimum bias data from Au+Au collisions, after applying the momentum dependent residual cut between the track projection point and TOF hits. Figure 7 shows the mass squared distribution for positively and negatively charged particles. The vertical axis is in arbitrary units. This figure demonstrates the clear particle identification capability by PHENIX TOF detector during the run 2000.

Figure 8 shows the Pt spectra of π° for most central collisions and then the result is compared with the WA98 π° spectra for the same centrality class. WA98 is a Pb+Pb fixed target heavy ion experiment with $\sqrt{s}_{NN} = 17.2$ GeV. The recent WA98 direct photon paper was published in ref. [18]. The PHENIX inverse slope is significantly larger than the WA98 result and reached the upper Pt limit of WA98.

High-P_{T} particle spectra from heavy ion collisions are calculated in a parton model [17,16] by Wang. It is predicted in the paper that QCD-initiated hard scattering and evolution in which intrinsic transverse momentum is broadened due to initial multiple parton scattering and there is jet quenching due to parton energy loss inside a dense medium.

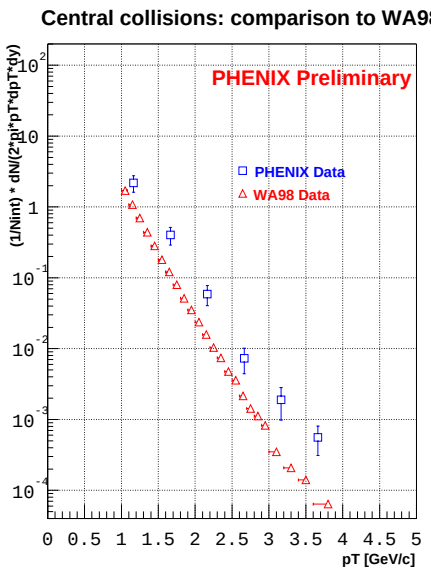

Figure 8. P_{T} spectrum of π° for 10% most central collisions for WA98 and PHENIX preliminary data. WA98 is a fixed target CERN, SPS experiment for Pb–Pb collisions with $\sqrt{s}_{NN} = 17.2$ GeV.

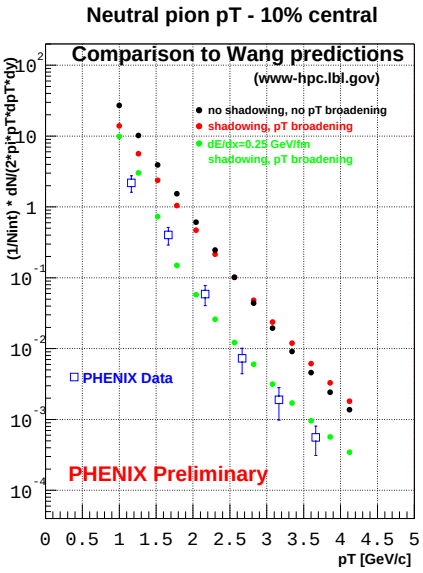

Figure 9. P_{T} spectrum of π° for 10% most central collision in PHENIX and a comparison is made with the Xin–Nian Wang's calculation.

Figure 9 shows the P_{T} spectra for preliminary PHENIX data and compared with the Wang's calculation. This is done in order to see if there is any effect by the propagation of partons in the dense medium. Data shows inconsistent with scenarios without $\mathrm{d}E/\mathrm{d}x$ loss and not inconsistent with $\mathrm{d}E/\mathrm{d}x = 0.25$ GeV/fm.

Figure 10 is illustrative of current evidence for strong elliptic flow [27] for charged particles detected at mid-rapidity ($-0.35 \leq \eta \leq 0.35$) for Au–Au collisions at $\sqrt{s}_{NN} = 130$ GeV. The preliminary data shown in the figure represent two-particle azimuthal correlation functions obtained for $0-5\%$ (top panel), $5-15\%$ (middle panel), and $15-30\%$ (bottom panel) centrality classes for charged particles with 0.5 GeV $< P_{\mathrm{T}} <$ 2.5 GeV. The correlation function is defined as $C(\Delta\Phi) = R(\Delta\Phi)/B(\Delta\Phi)$ where $R(\Delta\Phi)$ represents the $\Delta\Phi$ distribution of particle pairs obtained from the same event and $B(\Delta\Phi)$ represents the $\Delta\Phi$ distribution of uncorrelated pairs obtained by randomly selecting each member of a particle pair from different events having similar centrality and vertex position. The solid curves in figure 10 represent fits to the correlation function following the common Fourier analysis technique [28]. Such fits provide a measure of the magnitude of the elliptic flow via the v_2 Fourier coefficient. A clear increase in the anisotropy is observed in figure 10 with decreasing centrality from the correlation functions. That is, the anisotropy is the weakest for the most central collisions. This behavior constitutes one of the well known trends for elliptic flow [29,30] and can be attributed to an interplay between the geometry of the collision and the expansion dynamics of the high density participant matter.

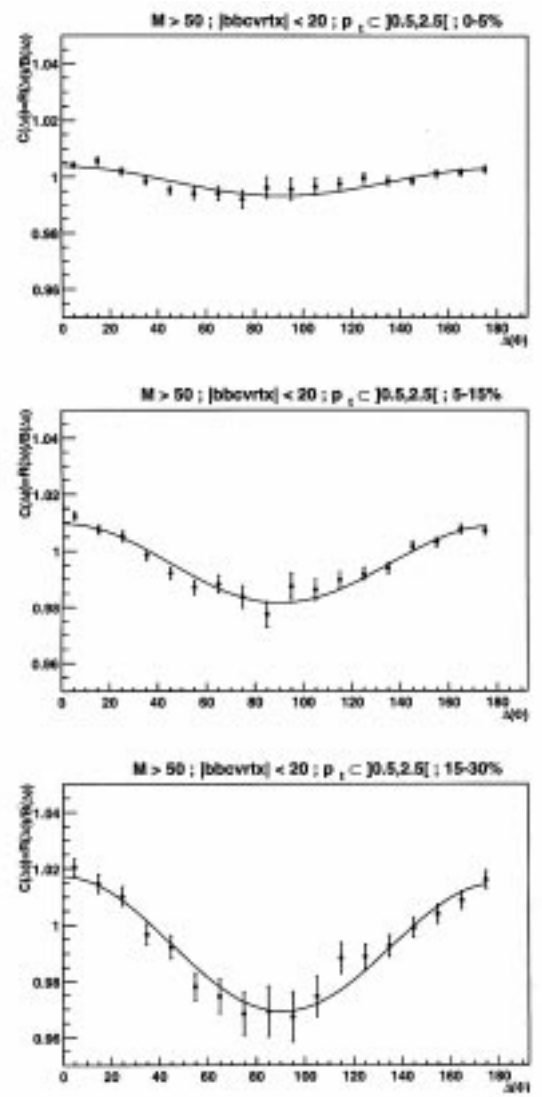

Figure 10. Azimuthal correlation functions are plotted for 0−5% (top panel), 5−15% (middle panel), and 15−30% (bottom panel) centrality classes from Au–Au collisions at $\sqrt{s}_{NN} = 130$ GeV. The $P_{\rm T}$ range is 0.5 GeV $< P_{\rm T} < 2.5$ GeV and pesudo-rapidity range is $-0.35 \leq \eta \leq 0.35$.

5. Summary

The spectrometers worked very well during the first PHENIX run at year 2000. The multiplicity distribution is consistent with the other RHIC experiment PHOBOS within the quoted errors. For the most central collisions the multiplicity per unit rapidity at $\eta = 0$

increases 80% from the SPS results. The mid-rapidity transverse energy density for central Au+Au collisions, and likely the spatial energy density, are more than 50% larger at $\sqrt{s_{NN}} = 130$ GeV (RHIC) than at $\sqrt{s_{NN}} = 17.2$ GeV (CERN). The striking increase of multiplicity density and $E_{\rm T}$ density per participant with centrality at RHIC must be confronted by the constancy of $\langle E_{\rm T}\rangle/\langle N_{\rm ch}\rangle$ at a value ~ 0.8 GeV observed both at RHIC and at CERN. Time-of-flight detector worked very effectively to identify e, π, K, p. PHENIX measured neutral pion Pt spectra betwen 1–4 GeV/c and this measurement is unique at RHIC. Results are not inconsistent with strong effects from the dense medium. The preliminary PHENIX data shows significant elliptical flow and the flow effect is stronger at the peripheral events than the central events.

Acknowledgements

We thank the staff of the RHIC project, Collider-Accelerator, and Physics Departments at BNL and the staff of PHENIX participating institutions for their vital contributions. We acknowledge support from the Department of Energy and NSF (USA), Monbu–sho and STA (Japan), Department of Atomic Energy (India), RAS, RMAE, and RMS (Russia), BMBF and DAAD (Germany), FRN, NFR, and the Wallenberg Foundation (Sweden), MIST and NSERC (Canada), CNPq and FAPESP (Brazil), IN2P3/CNRS (France), KRF and KOSEF (Korea), and the US–Israel Binational Science Foundation.

References

[1] The PHENIX Collaboration: D P Morrison, *Nucl. Phys.* **A638**, 565c (1998)
[2] J D Bjorken, *Phys. Rev.* **D27**, 140 (1983)
[3] E Kistenev *et al*, *Proceedings of the Fifth International Conference on Calorimetry in High Energy Physics* (World Scientific, 1994) pp. 211–223
[4] G David *et al*, *IEEE Trans. Nucl. Sci.* **45**, 692, 705 (1998)
[5] We used Woods-Saxon nuclear density distribution, Au nucleus radius $R = 6.65 \pm 0.3$ fm, diffuseness $a = 0.54 \pm 0.01$ fm and nucleon–nucleon cross section $\sigma_{nn} = 40 \pm 5$ mb
[6] WA98 Collaboration: M M Aggarwal et al, nucl-ex/0008004
[7] F Antinori *et al*, Preprint CERN-EP-2000-002
[8] PHOBOS Collaboration: B B Back *et al*, *Phys. Rev. Lett.* 85, 3100 (2000)
[9] NA49 Collaboration: F Siklér *et al*, *Nucl. Phys.* A661, 45c (1999)
[10] X N Wang and M Gyulassy, nucl-th/0008014
[11] K J Eskola, K Kajantie, P V Ruuskanen and K Tuominen, *Nucl. Phys.* **B570**, 379 (2000) and hep-ph/0009246
[12] e.g. see *Proc. Quark Matter 1987* edited by H Satz, H J Specht, R Stock, *Z. Phys.* **C38** (1988) pp. 1–370
Proc. Quark Matter 1999, edited by L Riccati, M Masera, E Vercellin, *Nucl Phys.* **A661**, pp. 1c–765c (1999)
[13] E802 Collaboration: T Abbott *et al*, BNL-67641 (August, 2000) submitted to *Phys Rev.*
[14] X N Wang and M Gyulassy, *Phys. Rev.* **D44**, 3501 (1991)
[15] NA49 Collaboration: T Alber *et al*, *Phys. Rev. Lett.* **75**, 3814 (1995)
[16] X N Wang and Z Huang, hep-ph/9701227
[17] X N Wang, *Phys. Rev.* **C61**, 064910 (2000)
[18] WA98 Collaboration, M M Aggarwal, *et al*, *Phys. Rev. Lett.* **85**, 3595 (2000)

[19] J-Y Ollitrault, *Phys. Rev.* **D46**, 229 (1992)
[20] P Danielewicz, *Phys. Rev.* **C51**, 716 (1995)
[21] H Sorge, *Phys. Rev. Lett.* **78**, 2309 (1997)
[22] D Teaney and E V Shuryak, *Phys. Rev. Lett.* **83**, 4951 (1999)
[23] WA93 Collaboration: M M Aggarwal *et al*, *Phys. Lett.* **B403**, 390 (1997)
[24] NA49 Collaboration: H Appelshäuser *et al*, *Phys. Rev. Lett.* **80**, 4136 (1998)
[25] WA98 Collaboration: M M Aggarwal *et al*, *Nucl. Phys.* **A638**, 459 (1998)
[26] E895 Collaboration: C Pinkenburg *et al*, *Phys. Rev. Lett.* **83**, 1295 (1999)
[27] STAR Collaboration: K H Ackermann *et al*, *Phys. Rev. Lett.* **86**, 402 (2001)
[28] A M Poskanzer and S A Voloshin, nucl-ex/9805001
[29] P F Kolb, J Sollfrank and U Heinz, nucl-th/9906003
[30] D Teaney, J Lauret and E V Shuryak, nucl-th/0011058
[31] G J Alner *et al*, *Z. Phys.* **C33**, 1 (1986)
[32] PHENIX Collaboration: K Adcox *et al*, *Phys. Rev. Lett.* **86**, 3500 (2001)